Tian Xia, Phillip R. Atkins, Wei E.I. Sha, and Weng C. Chew

Casimir Force

Vacuum fluctuation, zero-point energy, and computational electromagnetics.

The understanding of the Casimir force foretells applications in micro/nanoelectromechanical sensors and quantum friction. We review the history of quantum theory and Casimir force modeling and, using the homomorphism between electromagnetic oscillations and a linear pendulum with simple harmonic oscillation, we explore various concepts needed for Casimir force calculations. Through the argument principle, we simplify the derivation of Casimir energy and, hence, the Casimir force. Then, we discuss the connection between the Casimir force and computational electromagnetics (CEM), focusing on the method of moments (MOM). Finally, we consider the marriage of these concepts with recently developed broadband fast algorithms. The resulting approaches illustrate that the Casimir force calculation is for various highly complex structures.

Digital Object Identifier 10.1109/MAP.2021.3073118
Date of current version: 11 May 2021

INTRODUCTION

Quantum technologies have progressed by leaps and bounds in recent years. One of the more recent advances, the advent of a quantum computer by Google [1], heralds a new age for quantum technologies. As has been shown, quantum Maxwell's equations bear many similarities to classical Maxwell's equations. It is believed that many classical CEM methods can be used to solve quantum problems, as well. The Casimir force is one area where classical CEM can be applied to capture this quantum phenomenon. There could be more in the future [2], [3].

Quantum theory was conceived during the early part of the 20th century [2], [3]. A second wave of interest in it was aided by advances in nanofabrication and the validation of the new quantum interpretation by Bell's inequality in favor of the spooky nature of quantum theory in the 1980s [4]. In quantum theory, the state of a quantum system is indeterminate until after a measurement. Hence, information can be hidden in a quantum state until a measurement is performed on that state. This idea can be used for quantum

communication, forming an entirely secure way of transmitting information, thus ushering in an age of quantum information science.

To elaborate, a consequence of this is the idea of superposition: a quantum system is in a superposition of multiple states prior to a measurement. The resulting measurement determines what state the system is in. It also causes the collapse of the linear superposition of multiple states into the measured one. This enables a quantum system to have an infinite set of possibilities before certain measurements. As an example, the location of an electron, described by a wave function of the Hamiltonian, is indeterminate. It can be found anywhere the amplitude of the wave function is nonzero. The resulting measurement decides the location of the electron. In other words, the electron is in a linear superposition of states before the measurement. The measurement collapses the electron to the state that it finds. This behavior is not possible according the notion of classical particles; only "ghosts" and "angels" can do that [5].

The third bizarre concept of quantum theory is that of entanglement. For instance, due to momentum conservation, two photons generated from a single source have zero total angular momentum, even if they are traveling away from each other. Each is either right-hand circularly polarized (RHCP) or left-hand circularly polarized (LHCP), for a total sum of zero angular momentum. However, their state is unknown until there is a measurement. Before that, the quantum system is in a linear superposition of two photon states, where one of the photons is RHCP while the other is LHCP. When a measurement is performed on one of the photons to determine its polarization, the polarization of the other one is immediately known. For example, if one of the photons is measured to be LHCP, the other has to be RHCP. This is true even if the photons are miles apart, thus illustrating the nonlocality of quantum information. This indeterminacy of quantum information can be harnessed to increase diversity in a quantum state and is useful in quantum computers. Nonlocality is advantageous in quantum communication and quantum teleportation. This has caused quite a bit of excitement in the scientific community.

The Casimir force can be thought of as coming from zero-point energy and vacuum fluctuation fields (see Figure 1), which cause matter to be polarized and attracted to other matter. Hence, even at zero temperature, the attractive force is there. The experimental confirmation of the Casimir force was another boon to the validity of quantum theory, which refueled the interest in Casimir force studies [6]–[18]. One can think of the Casimir force as an extension of Van der Waal's forces. They exist in polar atoms and molecules because they polarize one another. When molecules become polar, their quiescent state is to move closer because that would decrease the potential energy of a system. Boltzmann's law states that a system would like to be in the lowest energy state. What happens if at zero temperature an atom or a molecule becomes neutral or nonpolar? The force due to polar molecules will disappear, as there are no fields to polarize them. Fortunately, quantum theory says that even at zero temperature, a vacuum-fluctuating field exists. This field polarizes neutral atoms and molecules, causing them to be attracted.

The Casimir force is a further generalization of Van der Waal's forces by accounting for quantum vacuum fluctuations and the retardation effect. Originally, a nonrelativistic quantum mechanical treatment of the problem generated the London force [19]. The vacuum fluctuation can be decomposed into Fourier components of different frequencies. Moreover, since the vacuum field is Maxwellian, it possesses a retardation effect. Casimir and Polder extended this treatment using quantum electrodynamic theory to allow for the consequences of retardation [20]. At low frequencies, these fields are in phase

or coherent with respect to each other, causing matter to be attracted. But at higher frequencies, the polarization of the matter gives rise to forces that are out of phase, or incoherent. Hence, the full model of the Casimir force that accounts for the retardation effect produces a force that is weaker than traditional Van der Waal's forces, as two objects are spaced farther apart. The force was experimentally confirmed in 1997 [6], which further affirmed the validity of quantum theory.

One of the more recent advances, the advent of a quantum computer by Google, heralds a new age for quantum technologies.

QUANTUM PENDULUM

To comprehend the concept of zero-point energy, it is best to understand the quantum pendulum [5], [21]–[28], which is homomorphic to quantum electromagnetic oscillations [29]. Thus, it is also easier to connect classical and quantum mechanics by using Hamitonian mechanics. A classical pendulum can be described by the Hamiltonian given by

$$H = \frac{p^2}{2m} + \frac{\kappa q^2}{2}, \tag{1}$$

where p and q are conjugate variables describing the momentum and position of the pendulum, respectively. The pendulum's equations of motion can be derived using Hamilton equations. These equations are derivable through energy conservation [28] and are

$$\frac{\mathrm{d}p}{\mathrm{d}t} = -\frac{\partial H}{\partial q}, \quad \frac{\mathrm{d}q}{\mathrm{d}t} = \frac{\partial H}{\partial p}. \tag{2}$$

By using (1), the right-hand side of (2) can be written more explicitly as

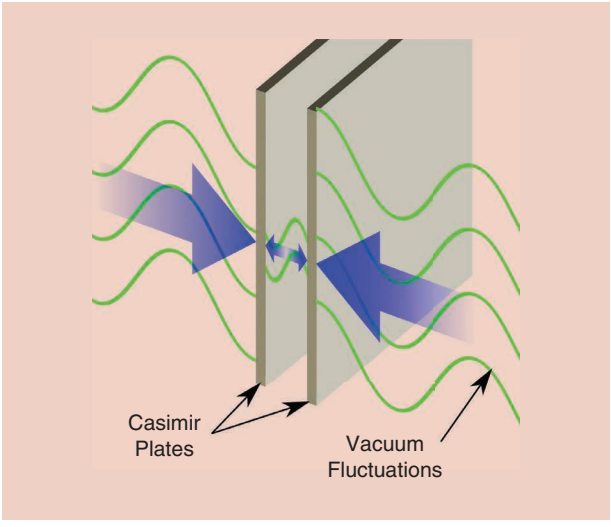

FIGURE 1. The Casimir force between two metal plates exists at $T = 0^{\circ}K$, due to the presence of a vacuum fluctuating field. (Source: Wikipedia.)

$$\frac{\mathrm{d}p}{\mathrm{d}t} = -\kappa q, \frac{\mathrm{d}q}{\mathrm{d}t} = \frac{p}{m}. \tag{3}$$

Combining the equation leads to

$$\frac{d^2q}{dt^2} = -\frac{\kappa}{m}q, \tag{4}$$

which is the classical equation of motion for a pendulum that has the oscillation frequency $\omega_0 = \sqrt{\kappa/m}$.

To derive the quantum equations of motion, the quantum Hamiltonian needs to be found [28]. It is obtained by elevating the conjugate variables p and q to become operators $\hat{p}$ and $\hat{q}$, respectively. By so doing, the corresponding Hamiltonian H also becomes an operator $\hat{H}$. For these operators to have meaning, they need to function on a quantum state $|\Psi\rangle$. The equation of motion of the quantum state $|\Psi\rangle$ is governed by the quantum state equation, which is

$$\hat{H}\,|\Psi\rangle = -i\hbar\partial_t\,|\Psi\rangle, \tag{5}$$

where $\partial_t = \partial/\partial t$. (This was originally postulated by Schrödinger and later used for other equations, including the Dirac equation [30]. This is analogous to the state-variable approach in control system theory [31].) When written explicitly, the preceding equation is

$$\left[\frac{\hat{p}^2}{2m} + \frac{1}{2}\omega_0^2 m\hat{q}^2\right]|\Psi\rangle = i\hbar\frac{\partial}{\partial t}|\Psi\rangle. \tag{6}$$

Furthermore, from energy conservation, the quantum Hamilton equation analogous to (2) can be derived [28]. Moreover, from the quantum state equation and quantum Hamilton equation, one can obtain the fundamental commutator

$$[\hat{q},\hat{p}] = i\hbar\hat{I}. \tag{7}$$

From this, it can be shown that

$$\hat{p} = -i\hbar\partial/\partial\hat{q}. \tag{8}$$

In the preceding, the derivative with respect to an operator has meaning if the operator is acting on its eigenvector [28], [29]. Using (8), the quantum state equation (6) can be explicitly rewritten as

$$\left[-\frac{\hbar^2}{2m}\frac{\partial^2}{\partial\hat{q}^2} + \frac{1}{2}\omega_0^2 m\hat{q}^2\right]|\Psi\rangle = i\hbar\frac{\partial}{\partial t}|\Psi\rangle. \tag{9}$$

When it is projected into the coordinate space, it becomes

$$\left[-\frac{\hbar^2}{2m}\frac{\partial^2}{\partial q^2} + \frac{1}{2}\omega_0^2 m q^2\right]\Psi(q,t) = i\hbar\frac{\partial}{\partial t}\Psi(q,t). \tag{10}$$

In this projection, we can think of $|\Psi\rangle$ as being expanded in terms of the eigenfunction of the $\hat{q}$ operator. The preceding is closer in form to the Schrödinger equation [2]. It can be solved by well-known partial differential equation techniques, such as the separation of variables. The solution can be written in terms of the product of Hermite-Gaussian functions and $\exp(-i\omega_n t)$, namely,

$$\Psi(q,t) = \Psi_n(q)\exp(-i\omega_n t). \tag{11}$$

By using this in (10), it can be shown that $\Psi_n(q)$ satisfies the equation

$$\left[-\frac{\hbar^2}{2m}\frac{d^2}{dq^2} + \frac{1}{2}\omega_0^2 m q^2\right]\Psi_n(q) = \hbar\omega_n\Psi_n(q). \tag{12}$$

Therefore, $\Psi_n(q)$, expressible in terms of Hermite-Gaussian functions, are eigenfunctions of the preceding equation, with the eigenvalues

$$E_n = \hbar\omega_n = \hbar\omega_0\left(n+\frac{1}{2}\right), \omega_n = \omega_0\left(n+\frac{1}{2}\right), \tag{13}$$

where $n = 0, 1, 2, \ldots$. In (13), E_n is the energy of the eigenmode. The lowest energy mode is

$$E_0 = \frac{1}{2}\hbar\omega_0, \tag{14}$$

which is the zero-point energy of the quantum pendulum. When this quantum pendulum is in thermal equilibrium with a bath, various modes of the quantum pendulum will be excited. The probability of the E_n mode being excited, according to Boltzmann's law [32], is proportional to

$$P_n \sim e^{-E_n/(k_B T)}, \tag{15}$$

where T is the temperature of the thermal bath and $k_B = 1.380649\times10^{-23}\,\mathrm{JK}^{-1}$ is the Boltzmann constant. Therefore, at $T = 0$, the quantum pendulum will be in its E_0 state, or the ground state. At the ground state, the quantum pendulum has zero mean in its oscillation and a nonzero mean square. That explains the ground state's nonzero energy. The pendulum has a fluctuating motion with zero mean and nonzero energy. The modes of an electromagnetic cavity are homomorphic to the quantum pendulums of different frequencies. Each of the modes has zero-point energy. Hence, the total zero-point energy of all the modes of a cavity is given by

$$\mathcal{E} = \sum_m \frac{1}{2}\hbar\omega_m, \tag{16}$$

where m is used to index different modes. The preceding is also called the *Casimir energy*, and, as will be shown, it is important for finding the Casimir force.

ARGUMENT PRINCIPLE

The argument principle for Casimir energy and the Casimir force was first used in 1968 [33], rarely with the MOM [34]. To illustrate it, we assume that $f(z)$ is analytic on and inside a closed contour C, except for finite poles and zeros inside C. In complex analysis, the argument principle (or Cauchy's argument principle) is given by

$$\oint_C dz\frac{f'(z)}{f(z)} = 2\pi i(Z-P), \tag{17}$$

where Z and P denote, respectively, the number of zeros and poles of $f(z)$ inside the contour C, with each zero and pole counted as many times as its multiplicity and order.

Equation (17) is useful for deriving the expression of Casimir energy, which can be represented as the sum of the mode energy at zero temperature, as in (16). Usually, the total energy needs to be renormalized since the summation in (16) diverges. Therefore, the renormalized Casimir energy can be written as [34], [35]

$$\mathcal{E} = \sum_m \frac{1}{2}\hbar\omega_m - \sum_n \frac{1}{2}\hbar\omega_n^{\mathrm{norm}}, \tag{18}$$

where ω_m is the system's mode frequencies and ω_n^{norm} is the normalization frequencies. We seek an alternate way to calculate the Casimir energy in (18). To this end, after changing the variable z to ω, we seek functions $f(\omega)$ and $f_{\mathrm{norm}}(\omega)$ such that $f(\omega_m) = 0$ and $f_{\mathrm{norm}}(\omega_n^{\mathrm{norm}}) = 0$ to the first order and with no poles in $f(\omega)$ and $f_{\mathrm{norm}}(\omega)$. Then the Casimir energy (18) can be rewritten as [35]

$$\mathcal{E} = \frac{\hbar}{4\pi i}\oint_C d\omega\omega\frac{d}{d\omega}\left(\ln\frac{f(\omega)}{f_{\mathrm{norm}}(\omega)}\right). \tag{19}$$

Using integration by parts, (19) becomes

$$\mathcal{E} = \frac{\hbar}{4\pi i}\oint_C d\omega\ln\frac{f(\omega)}{f_{\mathrm{norm}}(\omega)}. \tag{20}$$

To further simply the expression, we can construct an infinitely large semicircular contour C such that the integration along the infinity path vanishes due to Jordan's lemma:

$$\mathcal{E} = \frac{\hbar}{4\pi i}\int_{-\infty}^{\infty} d\omega\ln\frac{f(\omega)}{f_{\mathrm{norm}}(\omega)}. \tag{21}$$

Folding the integration to $0\to\infty$ and applying the Wick rotation,

$$\mathcal{E} = \frac{\hbar}{2\pi i}\int_0^{\infty} d\omega\ln\frac{f(\omega)}{f_{\mathrm{norm}}(\omega)}, \tag{22}$$

$$= \frac{\hbar c}{2\pi}\int_0^{\infty} d\kappa\ln\frac{f(ic\kappa)}{f_{\mathrm{norm}}(ic\kappa)}, \tag{23}$$

where we have let $\omega = ic\kappa$ (κ is a real number) for the ease of the Wick rotation. Equation (23) is an expression to calculate Casimir energy, with the integrand evaluated at imaginary frequencies, whose convergence property is greatly improved.

RELATION BETWEEN CEM AND THE MOM

The argument principle gives us a concise equation for finding the energy of these vacuum modes. Traditional CEM algorithms [36] can be used to define settings where the fluctuating fields satisfy the boundary conditions. Combined with the argument principle, a practical method of calculating the Casimir force by using the MOM arises.

MOM

The MOM [37] is a computational algorithm that is commonly employed in CEM and can solve for the fields scattered from

a set of objects due to an incident field. This can be used to solve for the radar cross section of aircraft, the performance of an antenna design, and electrical interference in a printed circuit board. A comprehensive explanation of the MOM can be found in [38]. In CEM, it is very common to discuss what is known as the *electric field integral equation* (*EFIE*) when exclusively dealing with perfect electric conductor (PEC) objects. The EFIE is derived from two simple conditions. The first is that given a set of source currents (these are impressed currents, as opposed to induced ones [39]), we can derive the resulting electric field via

$$\mathbf{E}(\mathbf{r},\omega) = i\omega\mu \int d\mathbf{r}' \overline{\mathbf{G}}(\mathbf{r},\mathbf{r}') \cdot \mathbf{J}(\mathbf{r}'), \tag{24}$$

where $\overline{\mathbf{G}}(\mathbf{r},\mathbf{r}')$ is the free space dyadic Green's function that relates a point source current to its resulting electric field. In essence, the electric field is the summation of the fields that arise when we represent the source currents as a collection of point sources.

The second stipulation is that PEC objects impose a boundary condition along their surfaces that requires the total tangential electric field to be zero. When solving for the fields scattered by an incident source, the total field is the summation of the incident and scattered fields. Equation (24) can be written more succinctly by using an integral operator $\mathcal{L}$::

$$\mathbf{E}(\mathbf{r}) = \mathcal{L}(\mathbf{r},\mathbf{r}') \cdot \mathbf{J}(\mathbf{r}'), \tag{25}$$

where integration across repeated variables is implied. By using the subspace projection method [22], [38], the preceding can be converted to a matrix equation:

$$\langle \mathbf{b}_i(\mathbf{r}), \mathbf{E}^i(\mathbf{r}) \rangle = \sum_{j=1}^{N} a_j \langle \mathbf{b}_i(\mathbf{r}), \mathcal{L}(\mathbf{r},\mathbf{r}') \cdot \mathbf{b}_j(\mathbf{r}') \rangle, \tag{26}$$

where $\mathbf{b}_i(\mathbf{r})$ are the basis and testing functions [38]. This becomes the matrix equation

$$\mathbf{V} = \overline{\mathbf{Z}} \cdot \mathbf{J}, \tag{27}$$

where $Z_{ij} = \langle \mathbf{b}_i(\mathbf{r}), \mathcal{L}(\mathbf{r},\mathbf{r}') \cdot \mathbf{b}_j(\mathbf{r}') \rangle$, $J_i = a_i$, and $V_i = \langle \mathbf{b}_i(\mathbf{r}), \mathbf{E}^i(\mathbf{r}) \rangle$. The vector V is the excitation vector, defined by the known incident electric field. The matrix $\overline{\mathbf{Z}}$ is called the impedance matrix and relates the scattered current vector $\mathbf{J}$ with its excitation. Thus, given the known excitation field, the scattered currents can be found via $\mathbf{J} = \overline{\mathbf{Z}}^{-1} \cdot \mathbf{V}$. The resulting coefficients can be used with basis functions to reconstruct the scattered currents and fields.

This idea can be used for quantum communication, forming an entirely secure way of transmitting information, thus ushering in an age of quantum information science.

THE MOM AND THE CASIMIR FORCE

The marriage of the MOM and other CEM techniques with the calculation of the Casimir force was developed in the Reid, Rodriguez, White, and Johnson method [40], [41]. However, a simpler and more general derivation can be performed by using the argument principle approach [34]. As we have seen, starting from the assumption that we can determine the eigenfrequencies of the field configurations that satisfy the boundary conditions imposed by the objects of interest, Casimir energy can be represented as in (23). The problem is thus to find some function $f(\omega)$ and its associated normalization $f_{\text{norm}}(\omega)$, taken as the geometry when the objects are infinitely separated, that evaluate to zero at the eigenfrequencies of the Casimir problem. If we were to imagine our objects inside a PEC cavity, the eigenfrequencies of interest would be the frequencies of the cavity modes, in other words, the frequencies where the electromagnetic fields satisfy the boundary conditions without any external sources. The use of a cavity and PEC objects was conducted in Casimir's first paper to calculate the Casimir force between two parallel, infinite, metallic plates [42].

Recall that the MOM, constructed from the boundary conditions imposed by PEC objects, gives us (27), which relates the excitation fields to the induced currents through a free-space dyadic Green's function that relates a point source current to the resulting electric field. In the case of the Casimir force, we wish to find the frequencies where currents can excite electric fields that satisfy the boundary conditions in the absence of any excitations. That is, we wish to find the frequencies where

$$\overline{\mathbf{Z}} \cdot \mathbf{J} = 0. \tag{28}$$

Since the impedance matrix is singular at these frequencies, we conclude that $f = \det \overline{\mathbf{Z}} = 0$ for the natural modes. In the case of enclosing our PEC objects inside a cavity, we would need only to adjust the matrix problem so that the dyadic Green's function relates a point source current to the resulting electric field. Then, we would take our cavity and expand its volume to the limit of infinity to represent free space. In doing so, we would arrive at the Casimir energy equation defined by (23) and (28), where the dyadic Green's function used in the impedance matrix is now the traditional free space dyadic Green's function with the imaginary frequencies used in the EFIE. The Casimir energy and force then become

$$\mathcal{E} = \frac{\hbar c}{2\pi} \int_0^\infty d\kappa \ln \frac{\det \overline{\mathbf{Z}}(\kappa)}{\det \overline{\mathbf{Z}}_\infty(\kappa)}, \tag{29}$$

$$\mathbf{F} = -\frac{\hbar c}{2\pi} \int_0^\infty d\kappa \nabla_i \ln \det \overline{\mathbf{Z}}(\kappa), \tag{30}$$

where ∇_i represents the derivatives with respect to the physical displacement of the ith object (the one we wish to find the forces acting upon). We can think of this as the change in the Casimir energy by perturbing the position of the object of interest. The integrand of the Casimir energy is found by solving for the eigenvalues of the impedance matrix generated with imaginary frequencies. Specifically (the following formula can be shown by using the fact that the determinant of a matrix is also the product of its eigenvalues [43]),

$$\ln\frac{\det\overline{\mathbf{Z}}(\kappa)}{\det\overline{\mathbf{Z}}_\infty(\kappa)}=\sum_{n=1}^{N}\ln\left(\frac{\lambda_n}{\lambda_n^\infty}\right), \tag{31}$$

where λ_n and λ_n^∞ are the eigenvalues of $\overline{\mathbf{Z}}$ and $\overline{\mathbf{Z}}_\infty$, respectively.

For the Casimir force, assuming that $\overline{\mathbf{Z}}$ is invertible, the integrand can be expressed as

$$\begin{aligned}\nabla_i \ln\det\overline{\mathbf{Z}}&=\frac{\nabla_i\det\overline{\mathbf{Z}}}{\det\overline{\mathbf{Z}}},\\&=\frac{\mathrm{tr}(\mathrm{adj}(\overline{\mathbf{Z}})\cdot\nabla_i\overline{\mathbf{Z}})}{\det\overline{\mathbf{Z}}},\\&=\mathrm{tr}(\overline{\mathbf{Z}}^{-1}\cdot\nabla_i\overline{\mathbf{Z}}),\end{aligned} \tag{32}$$

where the second equation is obtained from Jacobi's formula, which relates the gradient of the determinant of a matrix to the trace of the matrix. (Matrix $\overline{\mathbf{Z}}$ is singular at the resonance frequencies along the real axis. The original integration path encloses, but does not contain, these frequencies. After the Wick rotation, the integration path will be evaluated along the imaginary axis. Hence, it is a valid assumption.) The term $\mathrm{adj}(\overline{\mathbf{Z}})$ is the adjugate matrix $\overline{\mathbf{Z}}$: $\mathrm{adj}(\overline{\mathbf{Z}})=\det\overline{\mathbf{Z}}\cdot\overline{\mathbf{Z}}^{-1}$.

Therefore, the Casimir force can be expressed as the trace of a matrix or the sum of eigenvalues:

$$\begin{aligned}\mathbf{F}&=-\frac{\hbar c}{2\pi}\int_0^\infty d\kappa\,\mathrm{tr}(\overline{\mathbf{Z}}^{-1}(\kappa)\cdot\nabla_i\overline{\mathbf{Z}}(\kappa)),\\&=-\frac{\hbar c}{2\pi}\int_0^\infty d\kappa\sum_{n=1}^{N}\alpha_n,\end{aligned} \tag{33}$$

where α_n are the eigenvalues of the generalized eigenvalue problem

$$\nabla_i\overline{\mathbf{Z}}(\kappa)\cdot\mathbf{x}=\alpha\overline{\mathbf{Z}}(\kappa)\cdot\mathbf{x}. \tag{34}$$

By taking the Wick rotation and converting the impedance matrix to imaginary frequencies, we find that the integrand of the Casimir energy and force are concentrated in the low frequencies and that they quickly approach zero as the frequency increases. This makes it easy to use a Gauss–Laguerre quadrature rule to integrate in the imaginary frequency domain, enabling us to solve the impedance matrix by using a small number of frequencies to estimate the Casimir effect.

This behavior is not possible according the notion of classical particles; only "ghosts" and "angels" can do that.

To calculate $\overline{\mathbf{Z}}_\infty$, recall that its elements are defined as $Z_{ij,\infty}=\langle\mathbf{b}_i(\mathbf{r}),\mathcal{L}(\mathbf{r},\mathbf{r}')\cdot\mathbf{b}_j(\mathbf{r}')\rangle$, where $\mathbf{b}_i(\mathbf{r})$ represents the basis functions defined on the surface meshes of the objects. This defines an interaction of the source basis function $\mathbf{b}_j(\mathbf{r})$ to a response on the testing basis function $\mathbf{b}_i(\mathbf{r})$. If the objects were at infinite distances, no fields generated by currents on one object would reach the others. Thus, $Z_{ij,\infty}=0$ for pairs of bases that lie on different objects; otherwise, the entries will be the same as $\overline{\mathbf{Z}}$. Similarly, the matrix $\nabla_i\overline{\mathbf{Z}}$ will have only nonzero elements for the entries that represent interactions between the Casimir object of interest with another object. This makes the gradient matrix $\nabla_i\overline{\mathbf{Z}}$ have block diagonal matrices of zeros (since the block diagonal entries are interactions between basis functions on the same object). This means that $\nabla_i\overline{\mathbf{Z}}$ behaves as if it were preconditioned for the iterative eigenvalue solvers that are used in (34).

It is important to note that the underlying principle of this process is that we have defined a simple matrix equation that encapsulates the boundary conditions that must be satisfied and the fact that the fields must meet these conditions in the absence of an exciting source. A number of CEM algorithms apply to various conditions that can be used as direct substitutions for the preceding impedance matrix. The case of homogeneous bodies of dielectrics can be handled by methods such as the Poggio–Miller–Chang–Harrington–Wu–Tsai (PMCHWT) algorithm [44]. The cases of PEC and homogeneous dielectric bodies are handled by using surface integrals since the scattered currents can be restricted to the surfaces of the objects. Bodies of inhomogeneous materials can be managed through volumetric integral equations [45] and finite-element methods [46]–[48]. Another difficulty in CEM is using the MOM across all frequencies. At very low frequencies, certain mathematical problems arise that can be solved by a new impedance matrix defined by algorithms such as the augmented electric field integral equation [49]. All these algorithms can be used as direct replacements in the preceding analysis. As long as we keep the same general relationship of $\overline{\mathbf{Z}}\cdot\mathbf{J}=\mathbf{V}$, we can employ the argument principle to relate an algorithm to the Casimir force.

CASIMIR FORCE BETWEEN HIGHLY COMPLEX STRUCTURES

NUMERICAL ALGORITHM

As discussed, the Casimir force can be calculated with the MOM, which encapsulates the boundary condition of a system. As shown in (33), the inverse of the system matrix $\overline{\mathbf{Z}}$ and the derivative of $\overline{\mathbf{Z}}$ with respect to the displacement direction i are needed at the frequencies along the imaginary axis. The conversion to the imaginary frequencies is a result of the Wick rotation in (23), and it is motivated by the faster convergence in the evaluation of the integral [50]. Therefore, the integral in (33) can

be evaluated with the numerical integration method by using a few quadrature points:

$$F = -\frac{\hbar c}{2\pi}\sum_j w_j \operatorname{tr}(\overline{\mathbf{Z}}^{-1}(\kappa_j)\cdot\nabla_i\overline{\mathbf{Z}}(\kappa)), \tag{35}$$

where κ_j is the quadrature point along the imaginary axis and ω_j is the weighting factor.

Consider a problem with two objects; the matrix $\overline{\mathbf{Z}}$ can be written as a 2×2 block matrix:

$$\overline{\mathbf{Z}} = \begin{bmatrix} \overline{\mathbf{Z}}_{11} & \overline{\mathbf{Z}}_{12} \\ \overline{\mathbf{Z}}_{21} & \overline{\mathbf{Z}}_{22} \end{bmatrix}. \tag{36}$$

The evaluation of the term $\nabla_i\overline{\mathbf{Z}}$ can be simplified since only the interaction terms in the MOM matrix are needed. When the derivative is taken with respect to the displacement of the two objects, $\nabla_i\overline{\mathbf{Z}}_{11}$ and $\nabla_i\overline{\mathbf{Z}}_{22}$ vanish due to the fact that $\overline{\mathbf{Z}}_{11}$ and $\overline{\mathbf{Z}}_{22}$ are invariant with respect to the relative location of objects 1 and 2. Therefore,

$$\nabla_i\overline{\mathbf{Z}} = \begin{bmatrix} \overline{0} & \nabla_i\overline{\mathbf{Z}}_{12} \\ \nabla_i\overline{\mathbf{Z}}_{21} & \overline{0} \end{bmatrix}. \tag{37}$$

Apparently, when the direct method is used to solve for the integrand in (35), the complexity of the problem is then governed by the computation of $\overline{\mathbf{Z}}^{-1}$.

To avoid high complexity for large problems, we can apply fast algorithms. First, we notice that in (37) the diagonal blocks become zero, leaving only the interaction terms in the matrix. The matrix $\nabla_i\overline{\mathbf{Z}}$ becomes low rank if the two objects are far from each other since $\overline{\mathbf{Z}}_{12}$ and $\overline{\mathbf{Z}}_{21}$ are low rank. Still, if the matrix elements in $\overline{\mathbf{Z}}^{-1}$ need to be explicitly computed, the overall complexity is $O(N^3)$, where N is the size of matrix. Since the matrix in (37) is low rank, we can approximate it with the randomized singular value decomposition (rSVD) [51]:

$$\underbrace{\nabla_i\overline{\mathbf{Z}}}_{N\times N} \approx \underbrace{\overline{\mathbf{U}}}_{N\times k}\cdot\underbrace{\overline{\mathbf{\Sigma}}}_{k\times k}\cdot\underbrace{\overline{\mathbf{V}}^T}_{k\times N}, \tag{38}$$

where only the k largest singular values are kept and others are assumed to be small and ignored. In using the rSVD to factorize the matrix into the form shown in (38), it is necessary to calculate the matrix vector product $\nabla_i\overline{\mathbf{Z}}\cdot\mathbf{x}$, where $\mathbf{x}$ can be an arbitrary vector. Assuming that the flops count of the matrix vector product is $O(T)$, the total complexity of the decomposition in (38) is $O(4kT + 2k^2N)$.

Plugging (38) into (35), the expression of the Casimir force is

$$F = -\frac{\hbar c}{2\pi}\sum_j w_j \operatorname{tr}(\overline{\mathbf{Z}}^{-1}\cdot\overline{\mathbf{U}}\cdot\overline{\mathbf{\Sigma}}\cdot\overline{\mathbf{V}}^T). \tag{39}$$

We can then compute the product of the matrices from left to right. The first part, $\overline{\mathbf{X}} = \overline{\mathbf{Z}}^{-1}\cdot\overline{\mathbf{U}}$, can be calculated by solving the matrix equation with multiple right-hand sides defined in $\overline{\mathbf{U}}$:

$$\underbrace{\overline{\mathbf{Z}}}_{N\times N}\cdot\underbrace{\overline{\mathbf{X}}}_{N\times k} = \underbrace{\overline{\mathbf{U}}}_{N\times k}. \tag{40}$$

Two photons generated from a single source have zero total angular momentum, even if they are traveling away from each other.

The complexity of this step can be reduced by using an iterative solver, $O(CkT)$, where C is the average number of iterations and T is the complexity of a matrix vector product.

Then, we can easily compute

$$\underbrace{\overline{\mathbf{Y}}}_{} = \underbrace{\overline{\mathbf{X}}}_{N\times k}\cdot\underbrace{\overline{\mathbf{\Sigma}}}_{k\times k\ (\text{diagonal})}, \tag{41}$$

where $\overline{\mathbf{\Sigma}}$ is the diagonal matrix and the complexity is O(kN). Finally, the trace calculation is

$$\operatorname{tr}(\overline{\mathbf{Y}}\cdot\overline{\mathbf{V}}^T) = \sum_i^N\sum_j^k y_{ij}\cdot v_{ij}, \tag{42}$$

where i and j are the row and column indices in the matrices. The complexity is $O(kN)$. Assuming that the number of iterations is constant and independent of the matrix sizes, the overall dominant complexity is $O(kT + k^2N)$, governed by (38) and (40).

Noticing that in the matrix vector product in (38) and (40) the matrices are represented with the integral kernel of Green's function, $g(\mathbf{r},\mathbf{r}') = 1/4\pi|\mathbf{r}-\mathbf{r}'|e^{ik|\mathbf{r}-\mathbf{r}'|}$, we can use the fast multipole algorithm (FMA) to accelerate the matrix vector product. However, the conventional FMA is suitable for a real wavenumber k (or a complex k with a small imaginary part). When the wavenumbers become purely imaginary, as in the case of calculating the Casimir force, the FMA needs modifications for numerical stability. In this article, we leverage the new broadband stable FMA, namely, hybrid FMA, as proposed in [52], and extend it to imaginary frequencies. At purely imaginary frequencies, the wavenumber k is also purely imaginary since ϵ and μ are always real along the imaginary frequency axis. By writing $k = i\kappa$, Green's function expanded through the addition theorem can be rewritten as

$$\frac{e^{-\kappa r_{ab}}}{r_{ab}} \approx \kappa\sum_{l=0}^{L_m}(-1)^l(2l+1)i_l(\kappa d)k_l(\kappa r_{ab})P_l(\hat{\kappa}\cdot r_{ab}), \tag{43}$$

where i_l and k_l are the modified spherical Bessel function of the first kind and second kind, defined by the spherical Bessel function j_l and the spherical Hankel function of the first kind $h_l^{(1)}$ [53]:

$$j_l(kx) = i^l i_l(\kappa x), \tag{44}$$

$$h_l^{(1)}(kx) = -i^{-l}k_l(\kappa x). \tag{45}$$

The vectors satisfy $\mathbf{r}_{ij} = \mathbf{r}_{ab} + \mathbf{d}$, and P_l is the Legendre polynomial of order l. In (43), all the terms in the right-hand side are real, therefore eliminating the numerical errors of the complex values in j_l and $h_l^{(1)}$.

Following similar derivations in [52], one can find an expansion of Green's function with a hybridization of the plane (now the exponential) wave and multipoles:

$$\frac{e^{-\kappa r_{ij}}}{r_{ij}} \approx \underbrace{\kappa \int d^2\hat{\kappa} e^{-\boldsymbol{\kappa}\cdot\mathbf{r}_{ia}} \cdot \alpha(l_0, \boldsymbol{\kappa}, \mathbf{r}_{ab}) \cdot e^{-\boldsymbol{\kappa}\cdot\mathbf{r}_{bj}}}_{\text{plane wave expansion}} + \underbrace{\kappa(\beta(\kappa, \mathbf{r}_{ia}) \cdot \tilde{\tilde{\alpha}}(L_0, L_m, \kappa, \mathbf{r}_{ab}) \cdot \beta(\kappa, \mathbf{r}_{bj}))}_{\text{multipole expansion}}, \quad (46)$$

where the plane wave expansion term captures the contributions from $l = 0$ to L_0 in (43) and the multipole expansion term captures those from $l = L_0 + 1$ to L_m. In the plane wave expansion term, the translation operator $\alpha(l_0, \kappa, \mathbf{r}_{mn})$ can be written as

$$\alpha(L_0, \boldsymbol{\kappa}, \mathbf{r}_{ab}) = \frac{1}{4\pi} \sum_{l=0}^{L_0} (2l+1) k_l(\kappa r_{ab}) P_l(\hat{\kappa} \cdot \mathbf{r}_{ab}). \quad (47)$$

In the multipole expansion, the terms $\beta(\kappa, \mathbf{r}_{ia})$, $\tilde{\tilde{\alpha}}(L_0, L_m, \kappa, \mathbf{r}_{ab})$, and $\beta(\kappa, \mathbf{r}_{bj})$, which are the receiving pattern, translator, and radiation pattern, are represented as vectors and matrices. The elements are defined as

$$\beta_{l'm'}(\kappa, \mathbf{r}_{ia}) = 2\sqrt{\pi}(-1)^{l'} Y_{l'm'}(\theta_{ia}, \phi_{ia}) i_{l'}(\kappa r_{ia}), \quad (48)$$

$$\alpha_{L',L''}(L_0, L_m, \kappa, \mathbf{r}_{ab}) = \sum_{l=L_0+1}^{L_m} 4\pi \mathcal{A}_{L',L'',L} \times Y_{l,m''-m'}(\theta_{ab}, \phi_{ab}) k_l(\kappa r_{ab}), \quad (49)$$

$$\beta_{l''m'}(\kappa, \mathbf{r}_{bj}) = 2\sqrt{\pi}(-1)^{l''} Y^*_{l''m''}(\theta_{bj}, \phi_{bj}) i_{l''}(\kappa r_{bj}), \quad (50)$$

where $|l' - l''| \le l \le |l' + l''|$. It should be noted that for a very large κ, it is not necessary to calculate Green's function because the value vanishes.

To validate the proposed hybrid FMA at imaginary frequencies, the method is applied to the worst case, when the two points $\mathbf{r}_a$ and $\mathbf{r}_b$ reside on the corner of the box, as in Figure 2. Here, the field is calculated through the aggregation from the source point $\mathbf{r}_a$ to the center of the box, translation to the center of the other box, and then disaggregation to the field point. In this example, the distance between the two boxes is $D = 2a$. By applying the method to determine L_0 and L_m, as discussed in [52], the errors of the algorithm can be well controlled within a large range of $\kappa = \Im[k]$. As demonstrated in Figure 3, the target errors can be precisely achieved and controlled up to 10^{-8}.

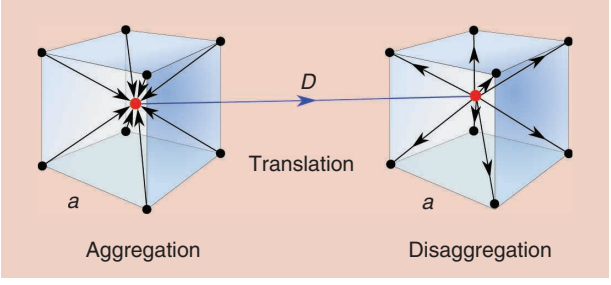

FIGURE 2. The worst-case one-level FMA calculations.

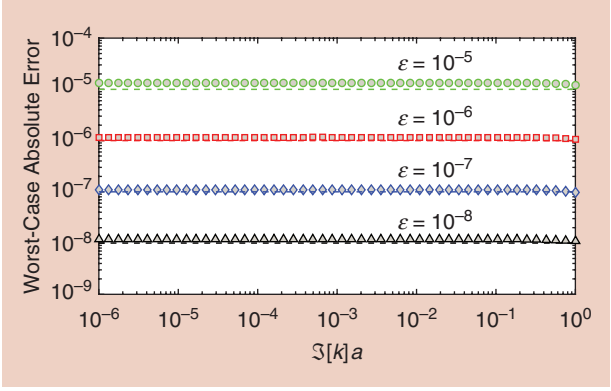

FIGURE 3. The worst-case absolute errors of the FMA with two buffer boxes at different $\Im[k]a$.

NUMERICAL RESULTS

In this section, we demonstrate the calculation of the Casimir force between various structures. We validate our method by comparing it with numerical and experimental results in the literature. More importantly, we simulate complex structures and find phenomena that have never been reported. The first example is a simple case, where two perfect conducting spheres (radius R = 1 nm) are displaced by distances $d = 0.1R, R$ and 2 R, as shown in Figure 4. (The conversion factor to nN is $\hbar c / R^2 \times 10^9$, which gives roughly 32 for R = 1 nm and 0.32 for R = 10 nm.)

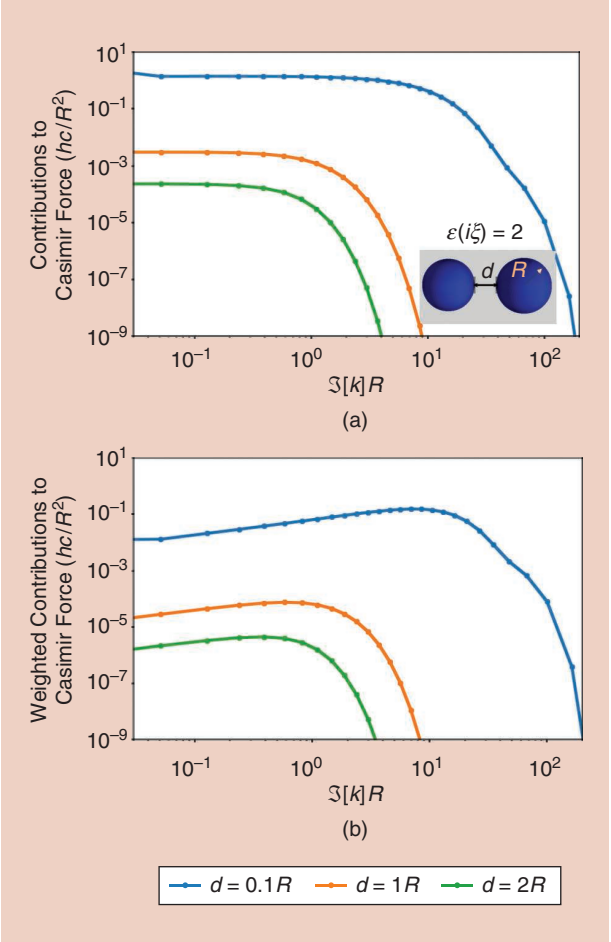

FIGURE 4. The contributions of the Casimir force at imaginary frequencies for two identical PEC spheres with a radius of R = 1 nm. (a) The trace $\mathrm{tr}(\overline{\mathbf{Z}}^{-1}(\kappa_j) \cdot \nabla_i \overline{\mathbf{Z}}(\kappa))$ evaluated at the imaginary wave numbers κ. (b) The weighted contributions $w_i \mathrm{tr}(\overline{\mathbf{Z}}^{-1}(\kappa_j) \cdot \nabla_i \overline{\mathbf{Z}}(\kappa))$ to the Casimir force.

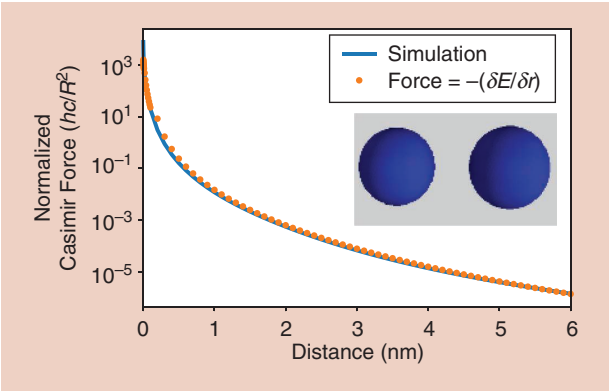

FIGURE 5. The simulation results of two PEC spheres compared to the differentiation of the Casimir energy reported in [40].

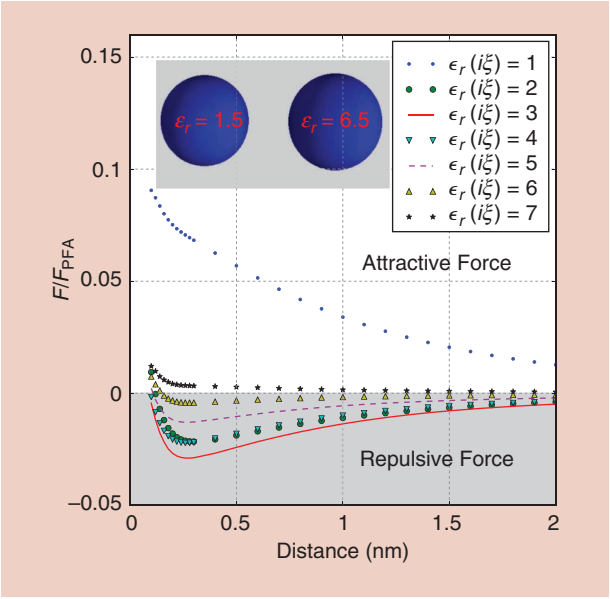

FIGURE 6. Attractive and repulsive forces between dielectric objects at different background permittivities.

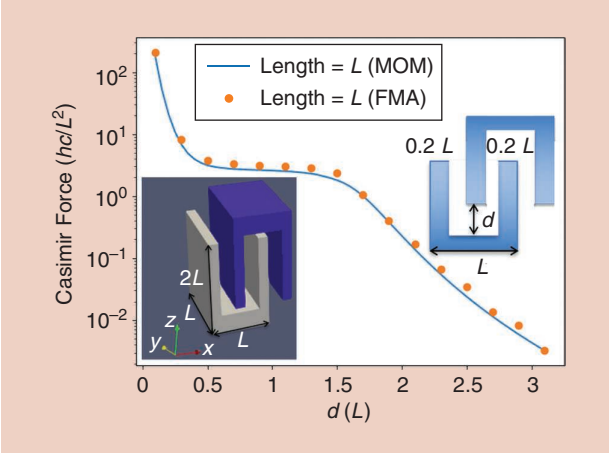

FIGURE 7. The repulse force between the two short U-shape PEC structures.

The MOM matrices are directly constructed using the EFIE. As illustrated in Figure 4, the contributions to the Casimir force dramatically decrease as the imaginary frequency κ increases, due to the increasing damping factor in Green's function. The numerical integration in (35) gives the net force between the two spheres, which is shown as the solid line in Figure 5. The results are validated by comparing them to the Casimir energy derivative in [40].

More interesting results appear in Figure 6 for two dielectric spheres submerged in different fluids. As suggested by Lifshitz's theory [54] and experimentally verified in [55], if the permittivity of the two objects and the fluid satisfies

$$\epsilon_1(i\xi) < \epsilon_{\text{fluid}}(i\xi) < \epsilon_2(i\xi), \tag{51}$$

the force between the two spheres becomes repulsive. In this numerical example, the permittivity of the spheres is fixed for all frequencies $\epsilon_1 = 1.5$ and $\epsilon_2 = 6.5$. The background permittivity is swept from one to seven, with a step of one. The amplitude of the force is normalized by proximity force approximation as

$$F_{\text{PFA}} = \frac{\pi^3 \hbar c R}{720 d^3}. \tag{52}$$

As shown in Figure 6, the repulsive force can be found when the relation in (51) is satisfied; i.e., $1.5 < \epsilon_{\text{fluid}} < 6.5$, while the force is always attractive for other ϵ_{fluid}.

In another example, we simulate a corrugated structure with all PEC materials, as in Figure 7. The height of the two identical U-shape structures is 2 L, where L is the width and length. In this simulation, we use the conventional MOM and the fast algorithm (rSVD plus the FMA) as a comparison. It can be seen that the two methods match well in terms of the amplitude of the Casimir force. The errors in the results of the fast algorithm are largely due to the truncated number of the singular values to factorize $\nabla_i \overline{\mathbf{Z}}$ and the residual errors in the iterative solver to find $\overline{\mathbf{Z}}^{-1}$. The outcomes are unsurprising since the direction of the force is always attractive.

In the next example, we found that a repulsive Casimir force can exist between PEC structures. A look-alike geometry reported in [56] shows repulsive forces for T-shaped protrusions. The effective repulsive force is a result of the attraction of the parts on the two bodies. In our example, given in Figure 8, the argument used in [56] cannot explain the existence of the repulsive force. Figure 8 is similar to Figure 7 but with a large height of 10 L and a width of 5 L. The lengths of the structures are 2 L and 10 L, as in Figure 9, so as to make multiple narrow cavities. The results in Figure 10 and Figure 11 document that the force changes its sign as d increases. The Casmir force is attractive when the distance d is small. As d increases, the force becomes repulsive and starts to oscillate between repulsive and attractive. In Figure 10, the Casimir force of the geometry in Figure 9 is compared, while the unit length Casimir force, scaled by factors of two and 10 respectively, is in Figure 11, where we can see that the amplitude of the force can be scaled by length.

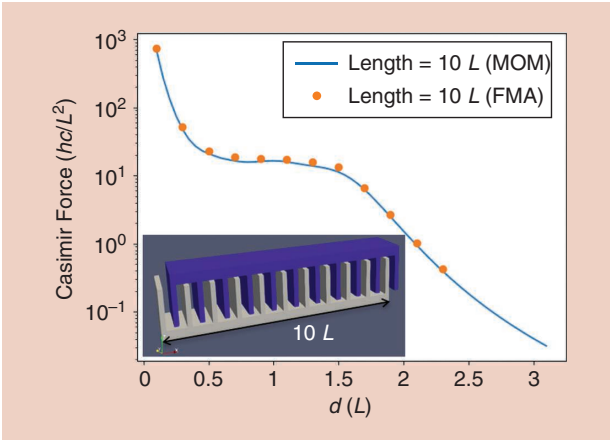

FIGURE 8. The repulse force between the two U-shape PEC structures.

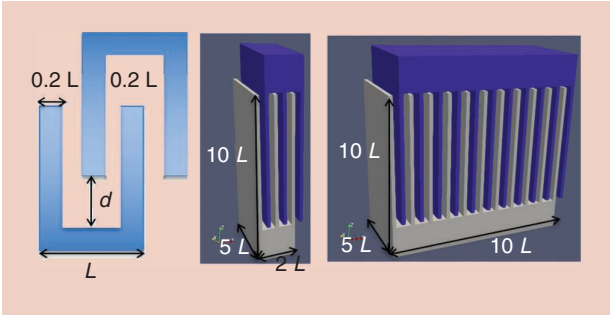

FIGURE 9. The geometry and dimensions of the two tall U-shape PEC structures.

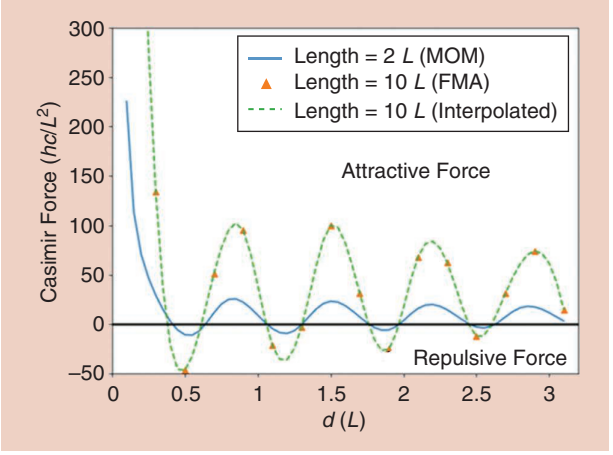

FIGURE 10. The attractive and repulsive forces as the displacement varies between the two tall U-shape PEC structures in Figure 9.

CONCLUSIONS

In this article, we have given a brief review of the quantum theory of the quantum pendulum, followed by a discussion of zero-point energy and vacuum fluctuation. We tried to present the topics in such a way that readers with knowledge of classical electromagnetics and some minimal understanding of quantum theory could follow them [57], [58]. We discussed the argument principle, which enables the calculation of the Casimir energy more easily from CEM. We illustrated this connection through the MOM. Using this simpler connection, we illustrated the computations of the Casimir force and Casimir energy for unprecedented, highly complex structures. We presented examples where a repulsive Casimir force can exist with PEC structures, in addition to attractive ones, which has never been shown before. The availability of repulsive forces in addition to attractive ones enables applications of Casimir analysis in microelectromechanical systems and nanoelectromechanical systems designs.

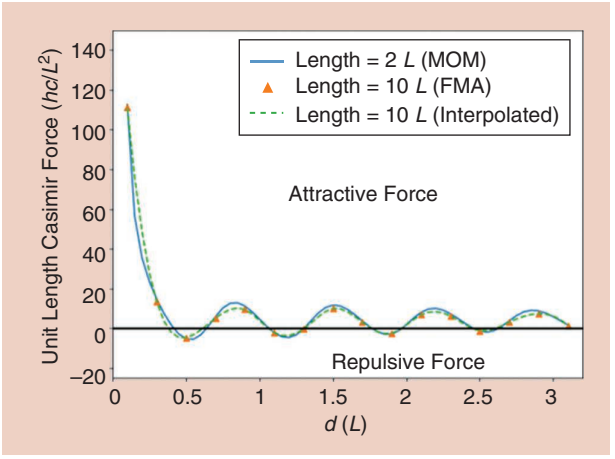

FIGURE 11. The normalized attractive and repulsive forces (the force per cavity) between the two tall U-shape PEC structures in Figure 9.

ACKNOWLEDGMENTS

This research was funded by the National Science Foundation, under grant 1818910, and a start-up fund at Purdue University. Weng C. Chew was supported by the Distinguished Visiting Scholars Scheme at Hong Kong University during the summer of 2019. Teaching assistance support from the University of Illinois at Urbana–Champaign is gratefully acknowledged.

AUTHOR INFORMATION

Tian Xia (tian_xia3@qq.com) is with Alibaba, Hangzhou, 31121, China. He received his Ph.D. degree from the University of Illinois at Urbana–Champaign.

Phillip R. Atkins (patkins@kla.com) is with KLA, Milpitas, California, 95035, USA. He received his Ph.D. degree from the University of Illinois at Urbana–Champaign.

Wei E.I. Sha (weisha@zju.edu.cn) is an assistant professor at Zhejiang University, Hangzhou, 310027, China. His research interests include computational electromagnetics, nonlinear electromagnetics, quantum electromagnetics, and topological electromagnetics. He is a Senior Member of IEEE.

Weng C. Chew (wcchew@purdue.edu) is a distinguished professor at Purdue University, West Lafayette, Indiana, 47907, USA. His research interests include computational and quantum electromagnetics, leading to more than 400 publications.

REFERENCES

[1] "Google claimed quantum supremacy in 2019 — and sparked controversy." ScienceNews. https://www.sciencenews.org/article/google-quantum-computer-supremacy-claim (accessed Nov. 1, 2019).

[2] E. Schrödinger, "An undulatory theory of the mechanics of atoms and molecules," *Phys. Rev.*, vol. 28, no. 6, p. 1049, 1926. doi: 10.1103/PhysRev.28.1049.

[3] P. A. M. Dirac, "The quantum theory of the emission and absorption of radiation," *Proc. Roy. Soc. A*, vol. 114, no. 767, pp. 243–265, 1927.

[4] A. Aspect, J. Dalibard, and G. Roger, "Experimental test of Bell's inequalities using time-varying analyzers," *Phys. Rev. Lett.*, vol. 49, no. 25, p. 1804, 1982. doi: 10.1103/PhysRevLett.49.1804.

[5] W. C. Chew, "Quantum mechanics made simple: Lecture notes," Univ. of Illinois, Urbana-Champaign, 2016. [Online]. Available: http://wcchew.ece.illinois.edu/chew/course/QMAll20161206.pdf

[6] S. K. Lamoreaux, "Demonstration of the Casimir force in the 0.6 to 6 μ m range," *Phys. Rev. Lett.*, vol. 78, no. 1, p. 5, 1997. doi: 10.1103/PhysRevLett.78.5.

[7] U. Mohideen and A. Roy, "Precision measurement of the Casimir force from 0.1 to 0.9 μ m," *Phys. Rev. Lett.*, vol. 81, no. 21, p. 4549, 1998. doi: 10.1103/PhysRevLett.81.4549.

[8] A. Lambrecht and S. Reynaud, "Casimir force between metallic mirrors," *Eur. Phys. J. D*, vol. 8, no. 3, p. 309, 2000. doi: 10.1007/s100530050041.

[9] H. Chan, V. Aksyuk, R. Kleiman, D. Bishop, and F. Capasso, "Quantum mechanical actuation of microelectromechanical systems by the Casimir force," *Sci.*, vol. 291, no. 5510, pp. 1941–1944, 2001. doi: 10.1126/science.1057984.

[10] M. Antezza, L. P. Pitaevskii, and S. Stringari, "Effect of the Casimir-Polder force on the collective oscillations of a trapped Bose-Einstein condensate," *Phys. Rev. A*, vol. 70, no. 5, p. 053619, 2004. doi: 10.1103/PhysRevA.70.053619.

[11] I. Brevik, J. Aarseth, J. S. Høye, and K. Milton, "Temperature dependence of the Casimir effect," *Phys. Rev. E*, vol. 71, no. 5, p. 056101, 2005. doi: 10.1103/PhysRevE.71.056101.

[12] B. E. Sernelius, "Casimir force and complications in the van Kampen theory for dissipative systems," *Phys. Rev. B*, vol. 74, no. 23, p. 233,103, 2006. doi: 10.1103/PhysRevB.74.233103.

[13] F. Capasso, J. N. Munday, D. Iannuzzi, and H. Chan, "Casimir forces and quantum electrodynamical torques: Physics and nanomechanics," *IEEE J. Sel. Topics Quantum Electron.*, vol. 13, no. 2, pp. 400–414, 2007. doi: 10.1109/JSTQE.2007.893082.

[14] S. Y. Buhmann, and and S. Scheel, "Thermal Casimir versus Casimir–Polder forces: Equilibrium and nonequilibrium forces," *Phys. Rev. Lett.*, vol. 100, no. 25, p. 253,201, 2008. doi: 10.1103/PhysRevLett.100.253201.

[15] A. Sushkov, W. Kim, D. Dalvit, and S. Lamoreaux, "Observation of the thermal Casimir force," *Nature Phys.*, vol. 7, no. 3, pp. 230–233, 2011. doi: 10.1038/nphys1909.

[16] R. Messina, P. A. M. Neto, B. Guizal, and M. Antezza, "Casimir interaction between a sphere and a grating," *Phys. Rev. A*, vol. 92, no. 6, p. 062504, 2015. doi: 10.1103/PhysRevA.92.062504.

[17] S. Y. Buhmann, *Dispersion Forces I: Macroscopic Quantum Electrodynamics and Ground-State Casimir, Casimir–Polder and van der Waals Forces*, vol. 247. Berlin: Springer-Verlag, 2013.

[18] P. W. Milonni, *The Quantum Vacuum: An Introduction to Quantum Electrodynamics*. San Francisco: Academic, 2013.

[19] F. London, "The general theory of molecular forces," *Trans. Faraday Soc.*, vol. 33, pp. 8b–26, Jan. 1, 1937. doi: 10.1039/tf937330008b.

[20] H. B. G. Casimir and D. Polder, "The influence of retardation on the London-van der Waals forces," *Phys. Rev.*, vol. 73, no. 4, pp. 360–372, 1948. doi: 10.1103/PhysRev.73.360.

[21] D. A. Miller, *Quantum Mechanics for Scientists and Engineers*. Cambridge, U.K.: Cambridge Univ. Press, 2008.

[22] W. C. Chew, "Electromagnetic field theory," Purdue Univ., West Lafayette, IN. [Online]. Available: https://engineering.purdue.edu/wcchew/ece604s20/EMFTAll.pdf

[23] M. O. Scully and M. S. Zubairy, *Quantum Optics*. College Park, MD: American Association of Physics Teachers (AAPT), 1999.

[24] L. Mandel and E. Wolf, *Optical Coherence and Quantum Optics*. Cambridge, U.K.: Cambridge Univ. Press, 1995.

[25] C. Gerry and P. Knight, *Introductory Quantum Optics*. Cambridge, U.K.: Cambridge Univ. Press, 2004.

[26] J. Garrison and R. Chiao, *Quantum Optics*. Oxford, U.K.: Oxford Univ. Press, 2008.

[27] R. Loudon, *The Quantum Theory of Light*. Oxford, U.K.: OUP Oxford, 2000.

[28] W. C. Chew, A. Y. Liu, C. Salazar-Lazaro, D. Na, and W. E. I. Sha, "Hamilton equation, commutator, and energy conservation," *Quantum Rep.*, vol. 1, no. 2, pp. 295–303, Dec 2019. doi: 10.3390/quantum1020027.

[29] W. C. Chew, A. Y. Liu, C. Salazar-Lazaro, and W. E. Sha, "Quantum electromagnetics: A new look–Part I," *IEEE J. Multiscale Multiphys. Comput. Techn.*, vol. 1, pp. 73–97, Oct. 12, 2016. doi: 10.1109/JMMCT.2016.2614800.

[30] P. A. M. Dirac, *The Principles of Quantum Mechanics*, no. 27. Oxford, U.K.: Oxford Univ. Press, 1981.

[31] D. E. Kirk, *Optimal Control Theory: An Introduction*. New York: Courier Corp., 2004.

[32] F. Reif, *Fundamentals of Statistical and Thermal Physics*, vol. 445. New York: McGraw-Hill, 1965.

[33] N. Van Kampen, B. Nijboer, and K. Schram, "On the macroscopic theory of van der Waals forces," *Phys. Lett. A*, vol. 26, no. 7, pp. 307–308, 1968. doi: 10.1016/0375-9601(68)90665-8.

[34] P. R. Atkins, Q. I. Dai, W. E. I. Sha, and W. C. Chew,c "Casimir force for arbitrary objects using the argument principle and boundary element methods," *Progress Electromagn. Res.*, vol. 142, pp. 615–624, 2013. doi: 10.2528/PIER13082105.

[35] P. R. Atkin, "A study on computational electromagnetics problems with applications to Casimir force calculations," Ph.D. dissertation, Univ. of Illinois, Urbana-Champaign, 2013.

[36] W. C. Chew, E. Michielssen, J.-M. Jin, and J. Song, *Fast and Efficient Algorithms in Computational Electromagnetics*. Norwood, MA: Artech House, 2001.

[37] R. F. Harrington, *Field Computation by Moment Methods*. New Jersey: Wiley-IEEE Press, 1993 (first edition 1968).

[38] W. C. Chew, M. S. Tong, and B. Hu, "Integral equation methods for electromagnetic and elastic waves," *Synthesis Lectures Comput. Electromagn.*, vol. 3, no. 1, pp. 1–241, Jan. 2008. doi: 10.2200/S00102ED1V01Y200807CEM012.

[39] R. F. Harrington, *Time-Harmonic Electromagnetic Fields*. New York: McGraw-Hill, 1961.

[40] M. H. Reid, A. W. Rodriguez, J. White, and S. G. Johnson, "Efficient computation of Casimir interactions between arbitrary 3D objects," *Phys. Rev. Lett.*, vol. 103, no. 4, p. 040401, July 20, 2009. doi: 10.1103/PhysRevLett.103.040401.

[41] M. H. Reid, J. White, and S. G. Johnson, "Computation of Casimir interactions between arbitrary three-dimensional objects with arbitrary material properties," *Phys. Rev. A*, vol. 84, no. 1, p. 010503, July 21, 2011. doi: 10.1103/PhysRevA.84.010503.

[42] H. G. Casimir, "On the attraction between two perfectly conducting plates," in *Proc. K. Ned. Akad. Wet.*, vol. 51, 1948, p. 793.

[43] G. H. Golub and C. F. van Loan, *Matrix Computations*, 4th ed. Baltimore: JHU Press, 2013.

[44] L. N. Medgyes-Mitschang, J. M. Putnam, and M. B. Gedera, "Generalized method of moments for three-dimensional penetrable scatterers," *J. Opt. Soc. Amer. A*, vol. 11, no. 4, pp. 1383–1398, 1994. doi: 10.1364/JOSAA.11.001383.

[45] W. C. Chew, *Waves and Fields in Inhomogeneous Media*. New York: Van Nostrand, 1990.

[46] J.-M. Jin, *The Finite Element Method in Electromagnetics*. Hoboken, NJ: Wiley, 2015.

[47] J. L. Volakis, A. Chatterjee, and L. C. Kempel, *Finite Element Method for Electromagnetics*. New Jersey: Wiley-IEEE Press, 1998.

[48] J.-F. Lee, R. Lee, and A. Cangellaris, "Time-domain finite-element methods," *IEEE Trans. Antennas Propag.*, vol. 45, no. 3, pp. 430–442, 1997. doi: 10.1109/8.558658.

[49] Z. G. Qian and W. C. Chew, "Fast full-wave surface integral equation solver for multiscale structure modeling," *IEEE Trans. Antennas Propag.*, vol. 57, no. 11, pp. 3594–3601, 2009.

[50] A. Rodriguez, M. Ibanescu, D. Iannuzzi, J. D. Joannopoulos, and S. G. Johnson, "Virtual photons in imaginary time: Computing exact Casimir forces via standard numerical electromagnetism techniques," *Phys. Rev. A*, vol. 76, no. 3, Sept. 2007. doi: 10.1103/physreva.76.032106.

[51] N. Halko, P. G. Martinsson, and J. A. Tropp, "Finding structure with randomness: Probabilistic algorithms for constructing approximate matrix decompositions," *SIAM Rev.*, vol. 53, no. 2, pp. 217–288, Sept. 2009. doi: 10.1137/090771806.

[52] T. Xia, L. L. Meng, Q. S. Liu, H. H. Gan, and W. C. Chew, "A low-frequency stable broadband multilevel fast multipole algorithm using plane wave multipole hybridization," *IEEE Trans. Antennas Propag.*, vol. 66, no. 11, pp. 6137–6145, Nov. 2018. doi: 10.1109/TAP.2018.2866535.

[53] M. Abramowitz and I. A. Stegun, *Handbook of Mathematical Functions: With Formulas, Graphs, and Mathematical Tables*, vol. 55. Courier Corp., 1965.

[54] E. M. Lifshitz, "The theory of molecular attractive forces between solids," *Sov. Phys.*, vol. 2, no. 1, pp. 73–83, 1956.

[55] J. N. Munday, F. Capasso, and V. A. Parsegian, "Measured long-range repulsive Casimir–Lifshitz forces," *Nature*, vol. 457, no. 7226, pp. 170–173, Jan. 2009. doi: 10.1038/nature07610.

[56] L. Tang et al., "Measurement of non-monotonic Casimir forces between silicon nanostructures," *Nature Photonics*, vol. 11, no. 2, pp. 97–101, Feb. 2017. doi: 10.1038/nphoton.2016.254.

[57] G. W. Hanson, "Aspects of quantum electrodynamics compared to the classical case," *IEEE Antennas Propag. Mag.*, vol. 62, no. 4, pp. 16–26, 2020. doi: 10.1109/MAP.2020.2990065.

[58] W. C. Chew, D. -Y. Na, P. Bermel, T. E. Roth, C. J. Ryu, and E. Kudeki, "Quantum Maxwell's equations made simple: Employing scalar and vector potential formulation," *IEEE Antennas Propag. Mag.*, vol. 63, no. 1, pp. 14–26, Feb. 2021. doi: 10.1109/MAP.2020.3036098.